Carbohydrate Polymers 96 (2013) 233–239

Contents lists available at SciVerse ScienceDirect

Carbohydrate Polymers

journal homepage: www.elsevier.com/locate/carbpol

Preparation and characterization of bionanocomposite films filled with nanorod-rich zinc oxide

Abdorreza Mohammadi Nafchi[a,*], Roghayeh Nassiri[a], Samira Sheibani[b], Fazilah Ariffin[b], A.A. Karim[b]

[a] Food Biopolymer Research Group, Food Science and Technology Department, Damghan Branch, Islamic Azad University, Damghan, Semanan, Iran
[b] Food Biopolymer Research Group, Food Technology Division, School of Industrial Technology, Universiti Sains Malaysia, 11800 Minden, Penang, Malaysia

ARTICLE INFO

Article history:
Received 9 February 2013
Received in revised form 2 March 2013
Accepted 16 March 2013
Available online 23 March 2013

Keywords:
Bionanocomposite
Zinc oxide nanorod
Antimicrobial activity
Oxygen permeability
Seal strength

ABSTRACT

The effects of zinc oxide nanorods (ZnO-nr) incorporation on the physical, mechanical, heat sealability, barrier, thermal and antibacterial properties of sago starch and bovine gelatin bionanocomposites films were investigated. The ZnO was incorporated into the films at different concentrations (1–5%, w/w total solid). All films were plasticized with 40% (w/w of total solid) of a combination of sorbitol/glycerol at 3:1 ratio. Incorporation of 5% of ZnO-nr to starch and gelatin films decreased the permeability to oxygen by 40% and 55%, respectively. Moisture content and water absorption capacity of the films were decreased by increasing the ZnO-nr contents. Mechanical and heat seal properties of the films were increased more than 20%. The films exhibited UV absorption and displayed an excellent antimicrobial activity against the *Escherichia coli*. These properties suggest that bionanocomposites based on ZnO-nr have the potential as an active packaging material for food and pharmaceutical industries.

1. Introduction

Over the past decade, the combination of nanoscale science and other technologies have been explored to develop various novel materials and applications (Narayanamurti, 2006). For example, incorporation of nanoparticles to composite materials to produce nanocomposite has generated a great deal of attention due to enhancement of polymer properties such as thermal, mechanical and gas barrier (Kurian, Dasgupta, Galvin, Ziegler, & Beyer, 2006).

Metal or metal oxides, particularly ZnO, TiO_2, MgO, and CaO, have attracted a great deal of attention (Fu et al., 2005) due to both stability under harsh condition processes and safe material for application in animals and human (Lin, Akil, & Mahmud, 2009).

Bionanocomposites as a new generation of nanocomposites represent the combination of a biopolymer and an inorganic material that shows at least one nanometer scale dimension (Darder, Aranda, & Ruiz-Hitzky, 2007). Bionanocomposites have been shown to exhibit enhanced thermal, mechanical, and functional properties due to nanoparticle fillers (Jia et al., 2006). Furthermore, biopolymer-based nanocomposites can be regarded as green technology and show the biocompatibility and biodegradability in various applications such as agriculture, packaging, and pharmaceutical technology (Ma, Chang, Yang, & Yu, 2009; Nafchi, Moradpour, Saeidi, & Alias, 2013; Shameli, Ahmad, & Yunus, 2010).

Development of biopolymer films is another emerging research area; studies using starch and gelatin have been widely reported. Starch is widely available for various food and non-food uses while gelatin is known as good film former especially in pharmaceutical industry. Sago starch, among other commercial starches, is relatively unknown and come from uncommon source (*Metroxylon sagu* palm tree) (Karim, Tie, Manan, & Zaidul, 2008).

The nanofillers have high surface energy and large specific surface area, giving rise to a strong interfacial interactions between polymer and the nanofillers and bring about a significant enhancement in the polymer properties (Kovačević, Vrsaljko, Lučić Blagojević, & Leskovac, 2008).

Zinc oxide nanoparticles as functional filler have been widely used as UV-absorbers in cosmetics, coating materials, pigments, and barrier enhancer in a number of industrial products (Kumar & Singh, 2008; Li et al., 2009; Yu, Cai, & Liu, 2004). In addition, zinc oxide nanoparticles have been reported to exhibit antimicrobial effects (Li et al., 2009; Li, Xing, Li, Jiang, & Ding, 2010; Zhang, Ding, Povey, & York, 2008). Zinc oxide is one of the five zinc compounds that are currently listed as generally recognized as safe (GRAS) by the U.S. Food and Drug Administration (21CFR182.8991). Also, Zinc oxide nanoparticles, which are nontoxic and biocompatible, have been utilized as drug carriers and medical filling materials (Lin et al., 2009b; Mirhosseini & Firouzabadi, 2012).

* Corresponding author. Tel.: +98 232 522 6003; fax: +98 232 522 2133.
E-mail addresses: fstiau@gmail.com, fstiau@damghaniau.ac.ir (A.M. Nafchi).

0144-8617/$ – see front matter © 2013 Elsevier Ltd. All rights reserved.
http://dx.doi.org/10.1016/j.carbpol.2013.03.055

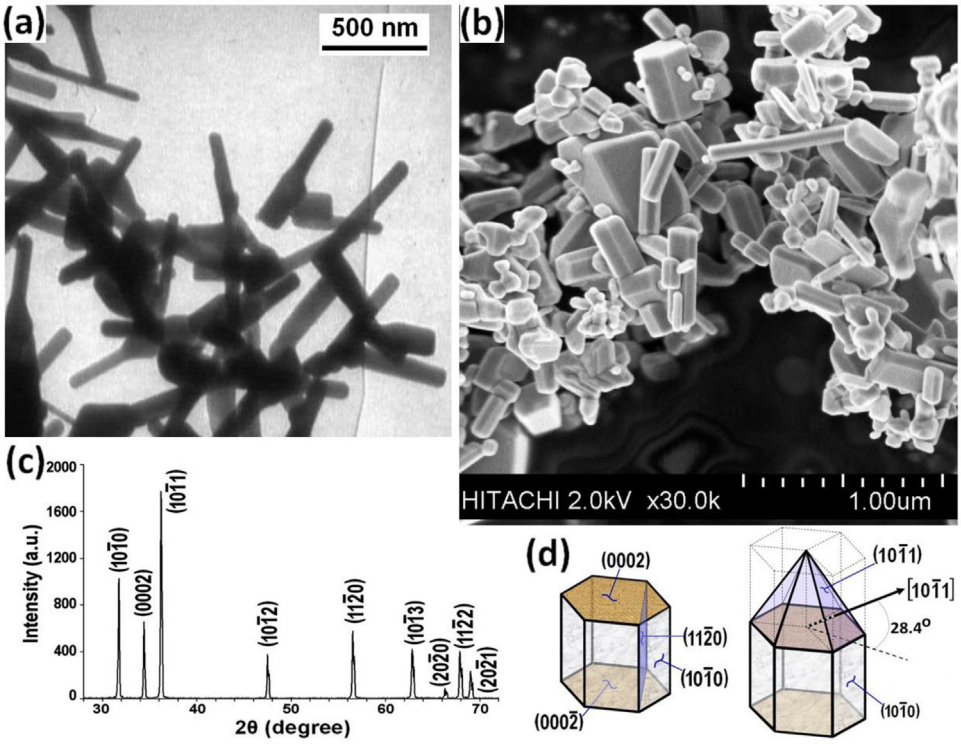

Fig. 1. (a) TEM micrograph of a cluster of ZnO nanorods (b) FESEM micrograph of nanorod-rich ZnO, (c) XRD spectrum of the ZnO, and (d) ZnO crystal simulation.

Generally the intrinsic properties of nanoparticles depend on the size, crystallinity, composition, morphology, and the shapes of the particles (Shahrom & Abdullah, 2006; Yamamoto, 2001). Nanorod shapes of Zinc oxide have been reported as the optimum shapes for UV-absorption activity (Lin et al., 2009b). Although some reports are available (Ma et al., 2009; Yu, Yang, Liu, & Ma, 2009) on the effect of ZnO nanoparticles incorporation on the starch film properties, to our knowledge ZnO nanorod-reinforced biopolymer films have not been investigated. It is hypothesized that by application of low concentration nanorod zinc oxide into the film, biopolymeric film with a UV shielding property can be produced for the edible and non-edible packaging industries.

In this paper, ZnO nanorods was used as a filler to prepare sago starch/ZnO-nr or gelatin/ZnO-nr bionanocomposites. The films were characterized for their antibacterial, physicochemical, mechanical, heat sealability, barrier, and thermal properties.

2. Materials and methods

2.1. Materials

Sago starch (31% amylose and 69% amylopectin) was purchased from SIM Company Sdn. Bhd (Penang, Malaysia) and bovine gelatin (Type B) was purchased from Sigma Chemical Co (St. Louis, MO, USA). Liquid sorbitol and glycerol were purchased from Liang Traco (Penang, Malaysia).

Zinc oxide nanorod (ZnO-nr) was synthesized from a method known as catalyst-free combust-oxidized mesh process. The properties and synthesis of ZnO-nr were fully described by Shahrom and Abdullah (2007). The structure of ZnO-nr powder is shown in the TEM and FESEM micrographs (Fig. 1(a) and (b)) that show ZnO-nr with 40–100 nm diameter and 200–700 nm length. Some micro-particles are also present but in smaller amount. The XRD spectrum in Fig. 1(c) shows four major crystal indices, (1 0 $\bar{1}$ 0), (0 0 0 2), (1 0 $\bar{1}$ 1) and (1 1 $\bar{2}$ 0), that form the ZnO rod crystal facets shown in the crystal simulations of Fig. 1(d).

Escherichia coli O157:H7 culture for antimicrobial assay was obtained from the culture collection center (School of Industrial Technology, Universiti Sains Malaysia, Malaysia). The bacterial culture was grown on nutrient agar slants and kept at 4 °C.

2.2. Preparation of nanobiocomposite films

ZnO-nr was dispersed in water at different concentrations (1, 2, 3, and 5%, w/w of total solid) and heated to 60 °C with continuous stirring for 1 h, then sonicated in an ultrasonic bath (Marconi model, Unique USC 45 kHz, Piracicaba, Brazil) for 30 min. The solution was cooled to room temperature and was used to prepare the aqueous starch dispersion 4% (w/w) and gelatin 8% (w/w). A mixture of sorbitol and glycerol (3:1) at 40% (w/w) of total solid was added as plasticizers. The choice of plasticizers and the concentration was based on Abdorreza, Cheng, and Karim (2011). The starch nanocomposites were heated to 90 ± 5 °C and held at this temperature for 45 min to complete the gelatinization whereas gelatin nanocomposites were heated to 58 ± 2 °C and held for 1 h. Upon completion of starch gelatinization, the solution was cooled to room temperature. The gelatin nanocomposite solution was cooled to 45 °C and the bubbles were removed by a laboratory scale vacuum pump.

A portion (90 g starch or 45 g gelatin) of the dispersion was cast on Perspex plates fitted with rims around the edge to yield a 16 × 16 cm^2 film-forming area. The films were dried under controlled conditions in a climatic chamber (25 °C and 50% RH). The control films were prepared with the same plasticizers but without addition of the nanoparticles. Dried films were peeled and stored at 23 ± 2 °C and 50 ± 5% relative humidity (RH) until tested. The thickness of each film was measured at five different locations and to the nearest 0.01 mm with a hand-held micrometer (Mitutoyo, Tokyo, Japan). All films (including control) were prepared in triplicate.

2.3. Characterizations

2.3.1. Moisture content

Moisture content of the films was determined using thermogravimetry analysis (TGA) (Pyris1 TGA, Perkin-Elmer, Massachusetts, USA) (Towns, 1995). The films were conditioned at 58% RH and 25 °C prior to analysis. The temperature of the TGA was increased from 25 °C to 130 °C at 3 °C/min, then held at 130 °C for 90 min. The change in weight (mass) of the samples was measured accurate to $\pm 10^{-3}$ mg. The mass loss was obtained after ensuring that the residual mass of the sample was constant.

2.3.2. Water absorption capacity

Water absorption capacity of the bionanocomposite films was measured with a method adapted from Kiatkamjornwong, Chomsaksakul, and Sonsuk (2000). Bionanocomposite films were first dried over phosphorous pentoxide for one week and then 50 mg of dried films was added to 100 mL of distilled water and allowed to stand for 30 min for swelling. The swollen films were filtered through steel screen (250-mesh) for 3 h and then drained films were weighed. The amount of water retained by the films per dried weight of the films was calculated as water absorption capacity.

2.3.3. Mechanical properties

ASTM D882-10 (ASTM, 2010) method was used to determine the mechanical properties under standard conditions. Film strips were cut to 100 mm long and 20 mm wide and conditioned at least for 48 h in 25 °C and 55% RH. Texture analyzer (TA.XT2, Stable Micro System, Surrey, UK) equipped with Texture Exponent 32 software V.4.0.5.0 was used for measuring mechanical properties of the films. The initial grip separation was 50 mm and crosshead speed was 0.5 mm/s. Elongation, Young's modulus, and tensile strength at break were calculated from the deformation and force data recorded by the software.

2.3.4. Heat seal strength measurement

Bionanocomposite films were cut and sealed according to the method described by Abdorreza et al. (2011). Seal strength of the heat-sealed films was determined according to standard ASTM F-88-09 (ASTM, 2009) using the TA.XT2 texture analyzer equipped with Texture Exponent 32 software V.4.0.5.0. Each leg of the sealed film was clamped to the texture analyzer, and each end of the sealed film was held perpendicular to the direction of the pull. The distance between the clamps was 2.5 cm. A 30-kg static load cell and a test speed of 60 mm/min were used. Seal strength (N/m) was calculated as the ratio of the maximum force required to cause seal failure to film width.

2.3.5. UV–visible (UV–vis)

The UV–visible for absorption spectrums of bionanocomposites films were recorded from 190 to 1100 nm using a UV–vis spectrophotometer model UV-1650PC (Shimadzu, Tokyo, Japan), using a blank glass plate as reference.

2.3.6. FTIR spectra

FTIR spectra of the films were recorded using an attenuated total reflection (ATR) method in Smart iTR (Thermo Scientific, Madison, USA). The thin films were applied directly onto the ZnSe ATR cell. For each spectrum, 64 consecutive scans at 4 cm^{-1} resolutions were averaged to reduce spectral noise.

2.3.7. Glass transition temperature by MDSC

The differential scanning calorimetry (DSC) analysis was performed using a modulated differential scanning calorimeter (DSC-Q100, TA Instruments, Newcastle, DE, USA) with refrigerator cooler. Calibration was done using pure indium and sapphire. An empty aluminum pan was used as a reference. The samples (10–20 mg each) were analyzed in modulation mode (MDSC). After equilibration at 0 °C, samples were heated at 2 °C/min (modulated at 60 s and amplitude 0.318 °C), up to 180 °C. The glass transition temperatures were determined from the resulting reverse heat flow thermograms as the midpoints between onset and end temperatures of step changes in heat flow observed during heating and identified as second-order transitions.

2.3.8. Oxygen permeability (OP)

Oxygen permeability measurements were performed on films with Mocon Oxtran 2/21 (Minneapolis, USA) equipped with a patented colometric sensor (Coulox®) and WinPermTM permeability software. The meaurements were done using the ASTM standard method D3985-05 (ASTM, 2005). The films were placed on an aluminum foil mask with an open area of 5 cm^2 and were mounted in diffusion cells. Tests were carried out at 25 °C temperature, atmospheric pressure, and 50% RH using 21% oxygen as test gas. Transferred oxygen through the films was conducted by the carrier (N_2/H_2) gas to the colometric sensor. Measurements were carried out on "convergent by hour" mode to reach the steady state of oxygen transmission. The permeability coefficients in cc-μm/(m^2 day atm) were calculated on the basis of oxygen transmission rate in steady state taking into account the films thickness.

2.3.9. Antimicrobial assay

Antimicrobial activity test on the films was carried out using the agar diffusion method according to Maizura et al. (2007). First, Mueller Hinton agar (Merk, Darmstadt, Germany) plates seeded with 0.2 mL of inoculums containing approximately 10^5–10^6 CFU/mL of *E. coli*. Then, film disks (6-mm diameter) placed on the plates. The plates were then incubated at 37 °C for 24 h. After that, the plates were examined for "zone of inhibition" of the film discs. Antimicrobial effects of the films were determined by calculating inhibition zone against *E. coli* O157:H7on solid media. The area of the whole zone was calculated and then subtracted from the film disk area, and this difference area was reported as zone of inhibition against *E. coli* O157:H7.

2.3.10. Statistical analysis

ANOVA and Tukey's Post Hoc tests were used to compare means of physical, mechanical, thermal, and antimicrobial properties of starch or gelatin films at the 5% significance level. Statistical analysis was conducted using PASW 18.0 for windows (SPSS Inc. Chicago, IL) and GraphPad Prism 5 (GraphPad Software Inc., La Jolla, USA).

3. Results and discussion

3.1. Moisture content

Moisture content of the films determined by TGA is shown in Table 1. Increasing the level of ZnO-nr caused the moisture content to decrease. It is likely due to the interaction among plasticizer, biopolymer matrix, and zinc oxide nanorods that reduced the hydroxyl group availability to interact with water, consequently leads to a less hygroscopic matrix. As reported by Müller, Laurindo, and Yamashita (2011) interactions occur between the ZnO and water and/or plasticizer of the ion-dipole type, that is, between the zinc and hydroxyl groups from the plasticizer and water.

3.2. Capacity to absorb water

Water absorption capacity of the ZnO-nr biocomposite films is given in Table 1. Introducing ZnO-nr to both gelatin and sago starch

Table 1
Moisture content and water absorption capacity (WAC) of sago starch and gelatin nanocomposite films.

Source	ZnO nanorod (%)	Moisture content (%) (at 58% RH)	WAC (g water/g dried film)
Sago Starch	0	12.26 ± 0.40a	2.50 ± 0.65a
	1	11.34 ± 0.30b	1.78 ± 0.18b
	2	10.88 ± 0.08c	1.74 ± 0.11b
	3	10.91 ± 0.04c	1.77 ± 0.10b
	5	10.61 ± 0.23c	1.32 ± 0.25c
Gelatin	0	14.88 ± 0.34A	9.93 ± 0.33A
	1	14.08 ± 0.14AB	8.50 ± 0.54B
	2	13.80 ± 0.23B	8.13 ± 0.44B
	3	13.31 ± 0.13C	7.19 ± 0.81C
	5	13.08 ± 0.13D	6.18 ± 0.62D

Values are mean ($n = 5$) ± SD. Different letters in each column represent significant difference at 5% level of probability among gelatin (capital letter) or sago starch films (small letter).

matrix significantly decrease the water absorption capacity of the biocomposites. This could be attributed to the interactions between ZnO and starch or gelatin in biopolymer film structure. The experimental results showed that when the nanoparticle (ZnO) content of films was increased, more hydrogen bonds formed between the ZnO and the matrix components (Tunç & Duman, 2010). For this reason, free water molecules do not interact as strongly as with nanocomposite films as with composite films alone. These results not only consistent with the moisture content results but also with results reported by other researchers on nanobiocomposites (Müller et al., 2011; Tunç & Duman, 2010).

3.3. Mechanical properties

Tensile strength (TS), elongation at break (E), Young modulus (YM), and heat seal strength of the bionanocomposite films are given in Table 2. As expected from other studies on biopolymer film reinforced by nanoparticles (Zou & Yoshida, 2010), significant increase was observed in TS and YM. In contrast, E was decreased by addition of ZnO-nr. There are two possible reasons for this phenomenon; the first is related to moisture content as discussed in the preceding section. On one hand, water can play a plasticizing role in the biopolymers matrix, and on the other hand, decreasing the plasticizer content decrease the flexibility of the films and consequently increasing the TS and YM and decrease the E (Cheng, Karim, & Seow, 2006; Müller et al., 2011; Nafchi, Alias, Mahmud, & Robal, 2012). The second reason is related to the interfacial interaction between ZnO-nr and biopolymer matrix. Mechanical properties of the composite films have been reported to be highly dependent

Table 2
Mechanical properties and heat seal strength of sago starch and gelatin nanocomposite films.

Source	ZnO nanorod (%)	Tensile strength (MPa)	Elongation at break (%)	Young modulus (GPa)
Sago starch	0	3.47 ± 0.34c	126.0 ± 1.8a	0.086 ± 0.016d
	1	5.19 ± 0.49b	122.5 ± 7.2a	0.107 ± 0.004c
	2	5.31 ± 0.32b	115.5 ± 12.3a	0.106 ± 0.004c
	3	5.45 ± 0.25b	101.4 ± 11.7b	0.135 ± 0.009b
	5	6.62 ± 1.02a	84.0 ± 16.9c	0.174 ± 0.008a
Gelatin	0	15.63 ± 0.74E	47.1 ± 5.8A	0.395 ± 0.042D
	1	17.07 ± 0.69D	31.6 ± 2.1B	0.407 ± 0.071C
	2	18.71 ± 0.85C	26.4 ± 4.5B	0.418 ± 0.019C
	3	19.39 ± 1.09B	32.0 ± 8.8B	0.442 ± 0.072B
	5	21.13 ± 1.52A	19.0 ± 4.9C	0.481 ± 0.045A

Values are mean ($n = 12$) ± SD. Different letters in each column represent significant difference at 5% level of probability among gelatin (capital letter) or sago starch films (small letter).

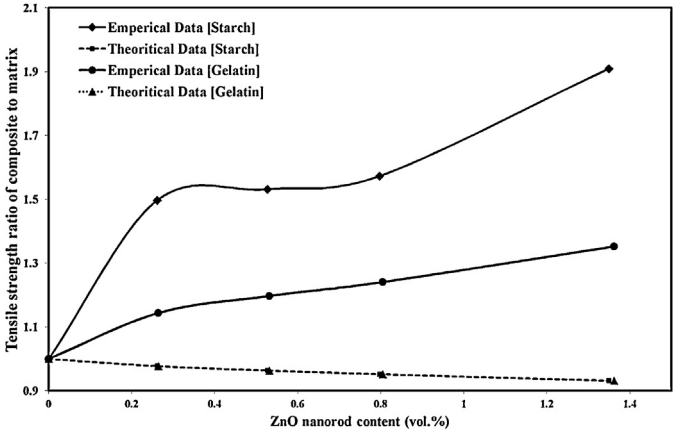

Fig. 2. Comparison of empirical (solid line) with theoretical (dashed line) data of tensile strength ratio of bionanocomposites to the respective matrix as a function of ZnO-nr volume fraction.

on the interfacial interaction between the matrix and fillers (Ma et al., 2009). Thus, theoretical tensile yield strength and experimental tensile strength of the composites were modeled for the cases of no adhesion and adhesion between the matrix and filler. If there is no adhesion, the interfacial layer cannot transfer stress. Nicolais–Narkis (Eq. (1)) model was used for predicting the theoretical tensile yield strength of the composites to evaluate the adhesion between the ZnO-nr and biopolymer matrixes (Ma et al., 2009).

$$\sigma_c = \sigma_m(1 - a\phi_f^b) \quad (1)$$

where Φ_f, σ_c, and σ_m are the volume fraction of the filler, and tensile strengths of the composite and biopolymer matrix, respectively. Parameters "*a*" and "*b*", in the Nicolais–Narkis model, are constants and related to the interaction of filler–matrix and the filler geometry, respectively. Values lower than 1.21 for "*a*" indicates good adhesion for composites. Eq. (2) for composites in the absence of adhesion will become (Metin, Tihminlioglu, Balköse, & Ülkü, 2004):

$$\frac{\sigma_c}{\sigma_m}(1 - 1.21\phi_f^{2/3}) \quad (2)$$

This prediction equation is based on the assumption that incorporation of nanoparticles caused the reduction in effective cross-section area and leads to decrease in the TS. In case of perfect adhesion between sago starch/gelatin and ZnO-nr, the loading stresses would be transferred to the ZnO-nr, and the effective cross-section area would not decrease. Fig. 2a and b shows the theoretical and experimental curves plotted for the effects of the volume fraction on TS ratio for sago starch and gelatin matrixes, respectively. The experimental values for both nanocomposite matrixes were much higher than those data predicted using Eq. (3). This suggests that there is a significant interaction between the gelatin or sago starch matrix and the ZnO-nr as filler.

3.4. Heat seal strength

The heat sealability is one of the critical factors for packaging materials but this aspect is less studied for biopolymeric films. Abdorreza et al. (2011) reported that plasticizers play a key role in starch films due to the enhanced hydrogen bonding between two surfaces to increase the seal strength. The seal strength for both gelatin and sago starch matrixes was increased by incorporation of lower percentage of ZnO-nr (Fig. 3). This increase was likely related to improvement of hydrogen and other bonds on the surface by ZnO-nr. However, the sealability of the films decreased with

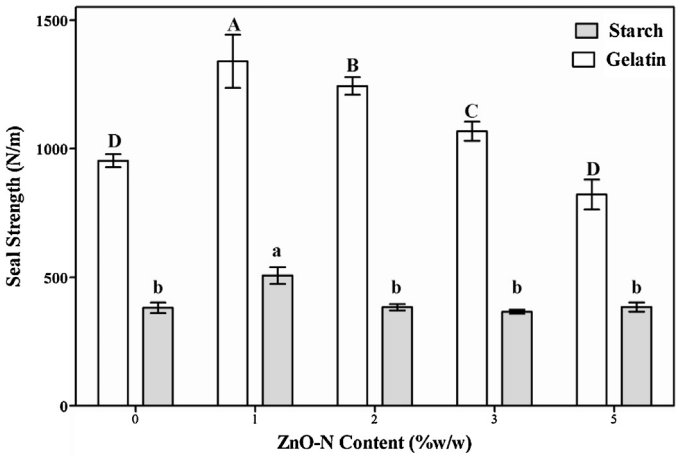

Fig. 3. Effects of ZnO-nr contents on heat sealability of gelatin and sago starch nanocomposite films. The bars show mean ($n = 8$) ± SD. Different letters on the bars represent the significant difference at 5% level of probability among gelatin (capital letter) or sago starch films (small letter).

addition of higher percentage of ZnO-nr, probably due to the reduction in moisture content and flexibility of the films (Abdorreza et al., 2011).

3.5. UV–visible (UV–vis) and FTIR spectra

Fig. 4(I) and (II) shows the UV–vis spectra of sago starch and gelatin films with different concentrations of ZnO-nr content, respectively. The absorption peak appeared at 375 and 380 nm for gelatin and sago starch/ZnO nanorod nanocomposites, respectively. This is in agreement with data reported by Subramani et al. (2007). The absorption peaks of these bionanocomposites exhibited an obvious blue-shift phenomenon. The blue shift is an emission of ZnO-nr biocomposites that can be attributed to the increased band gap of ZnO-nr as a result of the quantum confinement effect (Subramani et al., 2007). In both bionanocomposites films, by increasing ZnO-nr nanorod content, the peak absorption intensity and UV absorbance increased.

Yu et al. (2009) reported that addition of 5% of ZnO nanoparticles to the starch film increased the UV light absorption unit to 2.2, but in this study addition of lower percentage (2% for starch and 3% for gelatin) of the ZnO-nr absorbed the UV at the same level. The different behavior of ZnO-nr in the present study could be attributed to the morphology of the particles because according to the optimum shape for UV absorption is nanorod shape. The intense UV photocatalysis can also be attributed to the strong presence of the ionic crystal facets of (0 0 0 2) and (1 0 $\bar{1}$ 1) shown in Fig. 1; whereby these ionic crystal facets are highly excitonic at the UV near band-edge regime (Mahmud, 2011). This suggests that biopolymer matrix reinforced with ZnO-nr have potential for using as UV-shielding films.

The FTIR spectra of the gelatin nanocomposite matrix are shown in Fig. 4(III). There is no new functional group appears after application of ZnO, indicating that only physical interaction was involved between the ZnO-nr and the film matrix. Similar trend was seen for starch film (FTIR spectra not shown).

3.6. Glass transition temperature

Glass transition temperature (T_g) of the film materials is an important property in packaging industry. Modulated differential scanning calorimetry was used to determine the T_g of the films

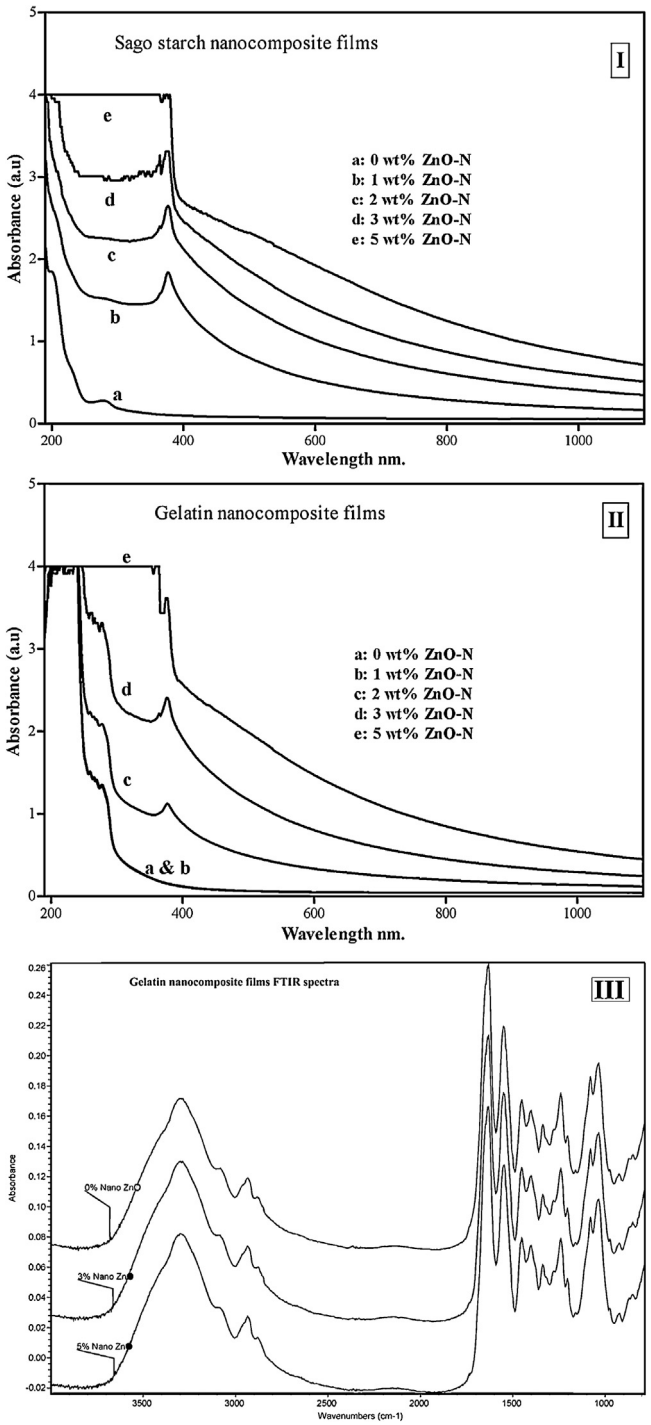

Fig. 4. UV–vis absorption spectra for (I) sago starch, (II) gelatin and (III) FTIR spectra for gelatin nanocomposite films at 25 °C.

due to the complexity of the biopolymer thermal properties. Fig. 5 shows reverse heat flow as a function of temperature for gelatin nanocomposites. The results indicate that addition of ZnO-nr significantly increased the T_g of the films from 59 to 63 °C. There is a negative relationship between moisture content and thermal properties of the biopolymer films (Abdorreza et al., 2011; Cheng et al., 2006). As discussed in the preceding section, moisture content of the films was decreased by addition of the ZnO-nr nanoparticles, consequently increase the T_g. Starch films also showed similar trend with T_g increased from 65 to 70 °C (data not shown).

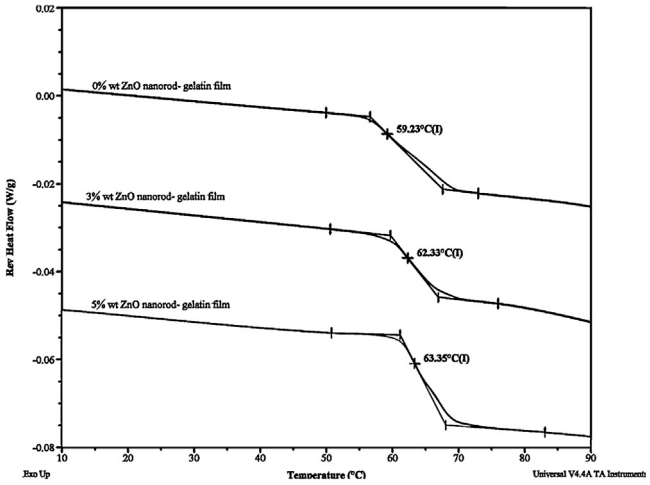

Fig. 5. Modulated differential scanning calorimetry graph of gelatin based nanocomposites.

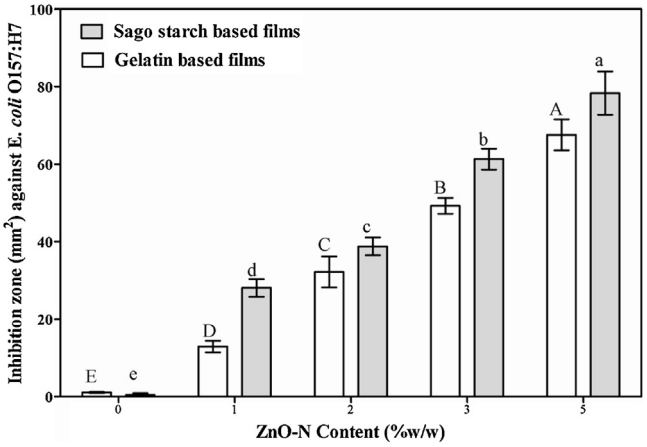

Fig. 6. Effects of ZnO nanorod contents on antimicrobial activity of gelatin and sago starch nanocomposite films. Inhibition zone = total inhibition area – total film area. The bars show mean ($n = 5$) ± SD. Different letters on the bars represent the significant difference at 5% level of probability among gelatin (capital letter) or sago starch films (small letter).

3.7. Permeability to oxygen

The results of oxygen permeability are presented in Table 3. Oxygen permeability coefficient significantly decreased by addition of ZnO-nr. The inorganic ZnO-nr particles are more water resistance than the biocomposite matrix; therefore incorporation of these nanorods to the matrix could likely introduced a tortuous pathway for oxygen molecules to pass through (Yu et al., 2009). Based on the Nielsen's (1967) simple model on tortuosity, it is possible to describe the permeability reduction in ZnO-nr incorporated biocomposites. He proposed that each layer of filler particles be positioned perpendicularly oriented to the diffusion pathway. The reduction in permeability coefficients means that oxygen should travel in a longer diffusive path. The relation between tortuosity and permeability as given by Nielsen's (1967) model is

$$\frac{P_c}{P_m} = \frac{1 - \varnothing_s}{\tau} \quad (3)$$

where τ is tortuosity, $\varnothing_s$ is the volume fraction of ZnO-nr, P_c and P_m are the permeability coefficients of the bionanocomposite and biocomposite, respectively. Table 3 shows the tortuosity value for each bionanocomposite matrix. The τ values for the gelatin nanocomposites are higher than those for sago starch, so decreasing in the permeability coefficients are higher for gelatin than starch. Zeppa, Gouanvé, and Espuche (2009) also reported similar results for oxygen permeability by incorporation of nanoparticles. The oxygen permeability of sago starch based films decreased from ~80 to ~50 cm^3 μm/(m^2 day atm), whereas for gelatin based films decreased from ~226 to ~105 cm^3 μm/(m^2 day atm).

Table 3
Oxygen permeability, and tortuosity value of sago starch and gelatin nanocomposites.

Source	ZnO nanorod (%)	O.P [cm^3 μm/(m^2 day atm)]	$O.P_{composite}/O.P_{matrix}$	τ
Sago Starch	0	79.88 ± 2.44a	1	1
	1	68.72 ± 1.28b	0.86	1.16
	2	56.98 ± 1.02c	0.71	1.39
	3	53.77 ± 0.50d	0.67	1.47
	5	48.20 ± 0.81e	0.60	1.64
Gelatin	0	226.18 ± 7.92A	1	1
	1	207.94 ± 7.34B	0.92	1.08
	2	154.54 ± 3.75C	0.68	1.46
	3	136.31 ± 3.60D	0.60	1.65
	5	104.59 ± 6.14E	0.46	2.13

Values are mean ($n = 5$) ± SD. Different letters in each column represent significant difference at 5% level of probability among gelatin (capital letter) or sago starch films (small letter). O.P, oxygen permeability coefficients at 20 °C and 50% RH; τ, tortuosity value from Nielson's equation.

3.8. Antimicrobial assay

Effects of film samples on the growth of *E. coli* were investigated. Fig. 6 shows the effects of ZnO-nr contents on antimicrobial activity of the different films. The inhibition zone of control and nano-incorporated films significantly was increased by increasing the ZnO-nr contents. Excellent antimicrobial activity of ZnO nanoparticles and the mechanism of the action against the microorganisms have also been demonstrated by other researchers (Li et al., 2009, 2010; Zhang et al., 2008).

Zhang et al. (2010) have been detailed the mechanisms of the antibacterial behavior of Zinc oxide. They have categorized this behavior as chemical and/or physical interaction between Zinc oxide particles and the cell envelope of microorganism. The Zn^{2+} could penetrate through the cell wall of microorganism and react with interior components that finally effects on viability of the cells. Another possible mode of action is generating of H_2O_2 due to presence of ZnO particles. Zhang et al. (2010) also reported that nano size of Zinc oxide is more effective than micro size due to easy penetration through cell wall of microorganisms. The nanorods could act as needle and easily penetrates through cell wall (Nafchi et al., 2012).

4. Conclusion

Nanorod-rich ZnO (ZnO-nr) was incorporated to the gelatin or sago starch matrixes to preparation of bionanocomposites. The special morphology of ZnO-nr plays a key role in the basic properties of the bionanocomposite matrixes. By incorporating low level of the filler (~2%), a huge differences between properties was observed especially in gas permeability and UV protection. On the other hand, Zinc is one of essential trace element, and if it is under regulation, the bionanocomposites based on ZnO-nr have an excellent potential application in medical, pharmaceutical, and food packaging.

Acknowledgement

We greatly thank and acknowledge Dr. Shahrom Mahmud for preparation of ZnO-nr and his technical supports.

References

Abdorreza, M. N., Cheng, L. H., & Karim, A. A. (2011). Effects of plasticizers on thermal properties and heat sealability of sago starch films. *Food Hydrocolloids*, *25*(1), 56–60.

ASTM. (2005). *Standard test methods for oxygen gas transmission rate through plastic film and sheeting using a coulometric sensor D 3985-05*. Philadelphia, PA: Annual Book of ASTM Standards.

ASTM. (2009). *Standard Test Method for Seal Strength of Flexible Barrier Materials F88/F88M-09*. Philadelphia, PA: Annual book of ASTM Standards.

ASTM. (2010). *Standard test method for tensile properties of thin plastic sheeting D882-10*. Philadelphia, PA: Annual book of ASTM standards.

Cheng, L. H., Karim, A. A., & Seow, C. C. (2006). Effects of water–glycerol and water–sorbitol interactions on the physical properties of konjac glucomannan films. *Journal of Food Science*, *71*(2), E62–E67.

Darder, M., Aranda, P., & Ruiz-Hitzky, E. (2007). Bionanocomposites: A new concept of ecological, bioinspired, and functional hybrid materials. *Advanced Materials*, *19*(10), 1309–1319.

Fu, L., Liu, Z., Liu, Y., Han, B., Hu, P., Cao, L., et al. (2005). Beaded cobalt oxide nanoparticles along carbon nanotubes: Towards more highly integrated electronic devices. *Advanced Materials*, *17*(2), 217–221.

Jia, W., Liu, C., Yang, L., Yang, J., Fan, L., Huang, M., et al. (2006). Synthesis, characterization, and thermal properties of biodegradable polyetheresteramide-based polyurethane. *Materials Letters*, *60*(29-30), 3686–3692.

Karim, A. A., Tie, A. P. L., Manan, D. M. A., & Zaidul, I. S. M. (2008). Starch from the sago (*Metroxylon sagu*) palm tree—Properties, prospects, and challenges as a new industrial source for food and other uses. *Comprehensive Reviews in Food Science and Food Safety*, *7*(3), 215–228.

Kiatkamjornwong, S., Chomsaksakul, W., & Sonsuk, M. (2000). Radiation modification of water absorption of cassava starch by acrylic acid/acrylamide. *Radiation Physics and Chemistry*, *59*(4), 413–427.

Kovačević, V., Vrsaljko, D., Lučić Blagojević, S., & Leskovac, M. (2008). Adhesion parameters at the interface in nanoparticulate filled polymer systems. *Polymer Engineering & Science*, *48*(10), 1994–2002.

Kumar, A. P., & Singh, R. P. (2008). Biocomposites of cellulose reinforced starch: Improvement of properties by photo-induced crosslinking. *Bioresource Technology*, *99*(18), 8803–8809.

Kurian, M., Dasgupta, A., Galvin, M. E., Ziegler, C. R., & Beyer, F. L. (2006). A novel route to inducing disorder in model polymer-layered silicate nanocomposites. *Macromolecules*, *39*(5), 1864–1871.

Li, J. H., Hong, R. Y., Li, M. Y., Li, H. Z., Zheng, Y., & Ding, J. (2009). Effects of ZnO nanoparticles on the mechanical and antibacterial properties of polyurethane coatings. *Progress in Organic Coatings*, *64*(4), 504–509.

Li, X. H., Xing, Y. G., Li, W. L., Jiang, Y. H., & Ding, Y. L. (2010). Antibacterial and physical properties of poly(vinyl chloride)-based film coated with ZnO nanoparticles. *Food Science and Technology International*, *16*(3), 225–232.

Lin, O. H., Akil, H. M., & Mahmud, S. (2009). Effect of particle morphology on the properties of nanoZnO/polypropylene composites. *Advanced Composite Letters*, *8*(3), 77–83.

Lin, W., Xu, Y., Huang, C.-C., Ma, Y., Shannon, K., Chen, D.-R., et al. (2009). Toxicity of nano- and micro-sized ZnO particles in human lung epithelial cells. *Journal of Nanoparticle Research*, *11*(1), 25–39.

Ma, X., Chang, P. R., Yang, J., & Yu, J. (2009). Preparation and properties of glycerol plasticized-pea starch/zinc oxide-starch bionanocomposites. *Carbohydrate Polymers*, *75*(3), 472–478.

Mahmud, S. (2011). One-dimensional growth of zinc oxide nanostructures from large micro-particles in a highly rapid synthesis. *Journal of Alloys and Compounds*, *509*(9), 4035–4040.

Metin, D., Tihminlioglu, F., Balköse, D., & Ülkü, S. (2004). The effect of interfacial interactions on the mechanical properties of polypropylene/natural zeolite composites. *Composites Part A: Applied Science and Manufacturing*, *35*(1), 23–32.

Mirhosseini, M., & Firouzabadi, F. B. (2012). Antibacterial activity of zinc oxide nanoparticle suspensions on food-borne pathogens. *International Journal of Dairy Technology*, http://dx.doi.org/10.1111/1471-0307.12015

Müller, C. M. O., Laurindo, J. B., & Yamashita, F. (2011). Effect of nanoclay incorporation method on mechanical and water vapor barrier properties of starch-based films. *Industrial Crops and Products*, *33*(3), 605–610.

Nafchi, A. M., Alias, A. K., Mahmud, S., & Robal, M. (2012). Antimicrobial, rheological, and physicochemical properties of sago starch films filled with nanorod-rich zinc oxide. *Journal of Food Engineering*, *113*(4), 511–519.

Nafchi, A. M., Moradpour, M., Saeidi, M., & Alias, A. K. (2013). Thermoplastic starches: Properties, challenges, and prospects. *Starch - Stärke*, *65*(1–2), 61–72.

Narayanamurti, V. (2006). Frontiers in nanoscience and technology in the 21st century and new models for research and education at the intersection of basic research and technology. *ASME Conference Proceedings*, *2006*(47608), 1203–1204.

Nielsen, L. E. (1967). Models for the permeability of filled polymer systems. *Journal of Macromolecular Science: Part A - Chemistry*, *1*(5), 929–942.

Shahrom, M., & Abdullah, M. J. (2006). Nanotripods of zinc oxide. In *IEEE conference on emerging technologies—nanoelectronics* 10–13 January, Singapore, (pp. 442–446).

Shahrom, M., & Abdullah, M. J. (2007). Tapered head of ZnO nanorods. *Journal of Solid State Science and Technology*, *15*(1), 108–115.

Shameli, K., Ahmad, M. B., & Yunus, W. M. Z. W. (2010). Green synthesis of silver/montmorillonite/chitosan bionanocomposites using the UV irradiation method and evaluation of antibacterial activity. *International Journal of Nanomedicine*, *5*(1), 875–887.

Subramani, C., Mhaske, S. T., Kathe, A. A., Varadarajan, P. V., Prasad, V., & Vigneshwaran, N. (2007). Functional behaviour of polypropylene/ZnO-soluble starch nanocomposites. *Nanotechnology*, *18*(38), 385702.

Towns, J. K. (1995). Moisture content in proteins: Its effects and measurement. *Journal of Chromatography A*, *705*(1), 115–127.

Tunç, S., & Duman, O. (2010). Preparation and characterization of biodegradable methyl cellulose/montmorillonite nanocomposite films. *Applied Clay Science*, *48*(3), 414–424.

Yamamoto, O. (2001). Influence of particle size on the antibacterial activity of zinc oxide. *International Journal of Inorganic Materials*, *3*(7), 643–646.

Yu, D., Cai, R., & Liu, Z. (2004). Studies on the photodegradation of Rhodamine dyes on nanometer-sized zinc oxide. *Spectrochimica Acta Part A: Molecular and Biomolecular Spectroscopy*, *60*(7), 1617–1624.

Yu, J., Yang, J., Liu, B., & Ma, X. (2009). Preparation and characterization of glycerol plasticized-pea starch/ZnO-carboxymethylcellulose sodium nanocomposites. *Bioresource Technology*, *100*(11), 2832–2841.

Zeppa, C., Gouanvé, F., & Espuche, E. (2009). Effect of a plasticizer on the structure of biodegradable starch/clay nanocomposites: Thermal, water-sorption, and oxygen-barrier properties. *Journal of Applied Polymer Science*, *112*(4), 2044–2056.

Zhang, L., Ding, Y., Povey, M., & York, D. (2008). ZnO nanofluids—A potential antibacterial agent. *Progress in Natural Science*, *18*(8), 939–944.

Zhang, L., Jiang, Y., Ding, Y., Daskalakis, N., Jeuken, L., Povey, M., et al. (2010). Mechanistic investigation into antibacterial behaviour of suspensions of ZnO nanoparticles against *E. coli*. *Journal of Nanoparticle Research*, *12*(5), 1625–1636.

Zou, D., & Yoshida, H. (2010). Size effect of silica nanoparticles on thermal decomposition of PMMA. *Journal of Thermal Analysis and Calorimetry*, *99*(1), 21–26.